Electronic Supplementary Material (ESI) for Inorganic Chemistry Frontiers.

Co-axial structure composed of RuO_2 on Defective N-doped Carbon Nanotubes as Highly Efficient Electrocatalyst for Overall Water Splitting

Wenqiang Li [a], Bowen Guo [ab], Ka Zhang [a], Heng Zhang [ac], Keqing Bu [a], Haipeng Chen [a], Xun Feng [*a]

a. College of Chemistry and Chemical Engineering, Luoyang Normal University, Luoyang, 471934, P. R. China, *E-mail: fengx@lynu.edu.cn*

b. College of Chemistry and Pharmaceutical Engineering, Nanyang Normal University, Nanyang, 473601, P. R. China

c. Science Island Branch of Graduate School, University of Science and Technology of China, Hefei, 230026, P. R. China

Experimental Section

1.1 Materials and reagent

Sodium tellurite (Na_2TeO_3, 99.5%, Alfa Aesar), melamine (99%, Acros Organics), hydrazine hydrate (N_2H_4, 64% v/v, Acros Organics), polyvinylpyrrolidone (PVP, K30, USB), sodium hydroxide (NaOH, Fisher Scientific), formaldehyde (37% v/v, Acros Organics), ammonia (NH_3, 35% in water, Acros Organics), ruthenium(III) chloride ($RuCl_3$, Strem Chemicals), and Pt/C (20 wt%, Alfa Aesar) were used as received without further purification. Water was supplied from a Barnstead Nanopure Water System (18.3 MΩ cm). RuO_2 was purchased from Aladdin company.

1.2 Synthesis Te NWs and Te-MF polymer core-sheath nanofibers

Te Nanowires (Te NWs) were prepared by a previous method.[1] Briefly, 0.5 g ascorbic acid (AA), 0.1 g CTAB and 56.9 mg Na_2TeO_3 were added to a beaker filled with 40 mL distilled water. The mixture moved into 50 ml autoclave and maintained at 90°C for 10 hours in an oven. Finally, the product was collected, washed and dried in a vacuum chamber for 10 h.

A certain of Te NWs and 0.126 g of melamine was dissolved in 25ml water and introduced into a 50 mL round-bottom flask. After 30 minutes under magnetic stirring, Te NWs solution which contained 20 μL 0.2M NaOH, and 0.53 mL formaldehyde were injected into the mixture solution, followed by stirring at 120 °C for another 10h. The product was obtained by filtration, washing with water and ethanol, is denoted as Te-MF (melamine–formaldehyde (MF) polymer coated onto the surface of Te NWs).

1.3 Material Characterization

The morphology of nanotubes can be observed by SEM (Hitachi S4800). All samples for the TEM analysis prepared by depositing a drop of the diluted suspension in ethanol on carbon film-coated copper grid. The high-resolution transmission electron microscopy (HRTEM, JEM-2010FEF) and a spherical aberration corrected Scanning Transmission Electron Microscope (AC-STEM, Titan G2 60-300 with image corrector) were conducted on an FEI TECNAI F20 microscope at an acceleration voltage of 200 kV. The crystal phase of as-prepared products was

determined by powder XRD using a PANalytical Empyrean, Netherlands X-ray diffractometer with Cu Kα radiation source. X-Pay photoelectron spectroscopy (XPS) measurements were performed with a VG Scientific ESCALAB 210 electron spectrometer using Mg KR radiation under a vacuum of 2×10^{-8} Pa at 14 KV.

1.4 Electrochemical Measurements

All electrochemical measurements were performed on CHI 660E electrochemical workstation in a standard 3-electrode with 2-compartment cell. A Glassy carbon electrode with 3mm diameter is working electrode. A saturated calomel electrode (SCE) is the reference electrode. A graphite plate or Pt wire was used as the counter electrode in HER test or OER electrochemical measurements. Polarization data were obtained at a scan rate of 5 mV s^{-1}. In all measurements, the reference electrode was calibrated with respect to reversible hydrogen electrode (RHE).

To prepare the catalyst ink, 5 mg catalyst powder was ultrasonically dispersed in 1000 μL mixed liquor (20 μL Nafion ionomer solution, 490 μL isopropanol and 490 μL deionized water). Then a certain amount of the dispersion was loaded onto a glassy carbon electrode with 3 mm diameter (loading 0.7 mg cm^{-2}). The obtained HER polarization curves were IR-compensated according to the following equation: $E_c = E_m - IR$ (where E_c is the IR-compensated potential, E_m is the experimentally measured potential, R is the solution resistance). The long-term stability was tested by a potentiation method at fixed potentials or a fixed current.

The catalyst RuO_2-DNCTs were loaded on GCE was used as both cathode and anode in a two-electrode configuration for overall water splitting. The LSV curves were obtained at a scan rate of 5 mV s^{-1} .The the chronopotentiometry experiment was conducted at 100 mA/cm^2 for 60 h.

The TOF (s^{-1}) values were calculated with the following equation:

TOF = I/mnF

I: Current (A) during the linear sweep voltammetry (LSV) tests in 1 M KOH.

n: Number of active sites (mol). F: Faraday constant (C mol^{-1}).

m: The factor 1/m represents that m electrons are required to form one H_2/O_2 molecule from water, which means that the m values for hydrogen evolution and oxygen evolution reactions are 2 and 4, respectively.

1.5 Theoretical calculation

Density functional theory (DFT) calculations were performed using a Dmol3 program package of software Materials Studio 7.0. The Perdew-Burke-Ernzerhof (PBE) function of the generalized gradient approximation (GGA) was used to account for electron exchange and correlation.[2] The computational parameters were self-consistent field (SCF) tolerance 1.0×10^{-7} Ha per atom, energy tolerance 2.0×10^{-7} Ha per atom, maximum force gradient 0.002 Ha $Å^{-1}$, maximum atomic displacement 0.005 Å, orbital cutoff 4.6 Å and thermal smearing 0.05 Ha for quick convergence. The supercells were relaxed with a $3 \times 3 \times 1$ Monkhorst-Pack k-mesh.

The four sequential electron transfer steps, including adsorption steps (i and iii), dissociation steps (ii and iv) and desorption step (v). Considering that the overall water decomposition process requires energy 4.92 eV at the standard conditions, the energy for at least one step in (i–iv) should be larger or equal to 1.23 eV. For the OER in alkaline environment, the whole process occurs via the following four elementary steps:

$$OH^- + * \rightarrow OH^* + e^- \quad (1)$$

$$OH^* + OH^- \rightarrow O^* + H_2O + e^- \quad (2)$$

$$O^* + OH^- \rightarrow OOH^* + e^- \quad (3)$$

$$OOH^* + OH^- \rightarrow O_2 + H_2O + e^- \quad (4)$$

The adsorption free energies (ΔG) of OER intermediates can be obtained by $\Delta G_i = \Delta E_i + \Delta ZPE_i - T\Delta S_i$, where i means OH*, O* and OOH*. Li et al. previously reported that ΔZPE - TΔS are 0.06, 0.37 and 0.44 eV for O*, OH* and OOH*, respectively.[3] Furthermore, the ΔE for OER intermediates was calculated as follow:

$$\Delta E_{OH} = E(OH^*) - E(^*) - [E(H_2O) - 1/2E(H_2)]$$

$$\Delta E_O = E(O^*) - E(^*) - [E(H_2O) - E(H_2)]$$

$$\Delta E_{OOH} = E(OOH^*) - E(^*) - [2E(H_2O) - 3/2E(H_2)]$$

Therefore, the Gibbs free energy changes for the four elementary steps of OER can be expressed as follows:

$$\Delta G_1 = \Delta G_{OH} - eU$$

$$\Delta G_2 = \Delta G_O - \Delta G_{OH} - eU$$

$$\Delta G_3 = \Delta G_{OOH} - \Delta G_O - eU$$

$$\Delta G_4 = 4.92\ eV - \Delta G_{OOH} - eU$$

Where U is the potential measured against the normal hydrogen electrode (NHE) at standard conditions. Therefore, the theoretical overpotential (η) for OER can be obtained by the following equation:

$$\eta_{OER} = \max[\Delta G_1, \Delta G_2, \Delta G_3, \Delta G_4]/e - 1.23\ [V]$$

The adsorption energy was calculated as [4]:

$$E_{ads} = E_{system} - [E_{slab} + E_{molecule}] \quad (5)$$

E_{system} is the total energy of the optimized system, E_{slab} is the total energy of the bare slab and $E_{molecule}$ is the total energy of an isolated RuO_2 or H_2O molecule.

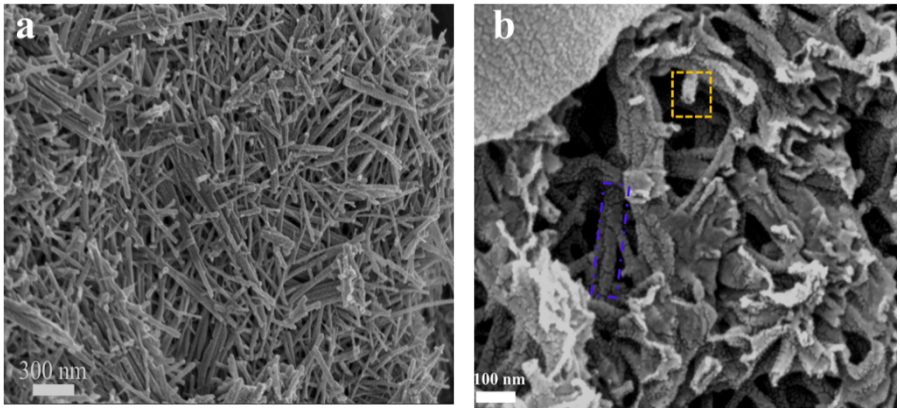

Fig. S1 (a-b) SEM image of Te nanowires and DNCTs.

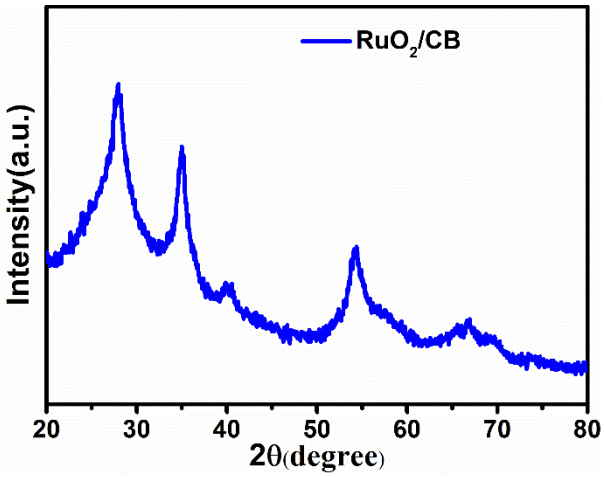

Fig. S2 XRD pattern of RuO_2/CB.

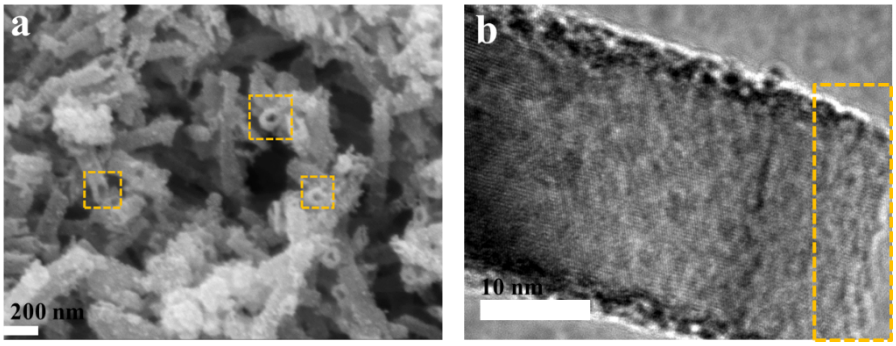

Fig. S3 SEM and TEM images of RuO_2-DNCTs.

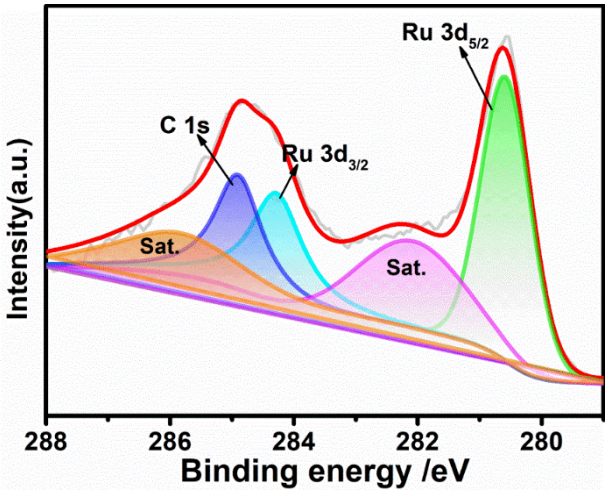

Fig. S4 High-resolution XPS spectra of Ru 3d in RuO_2-DNCTs.

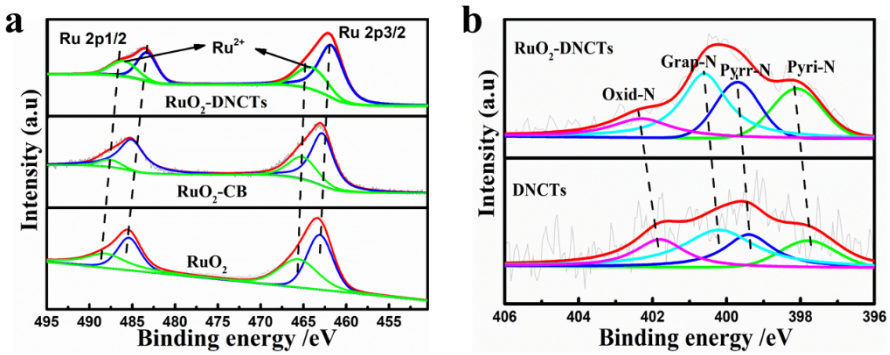

Fig. S5 (a) High-resolution XPS spectra of Ru 2p in RuO_2-DNCTs , RuO_2/CB and RuO_2, (b) High-resolution XPS spectra of N 1s in RuO_2-DNCTs and DNCTs.

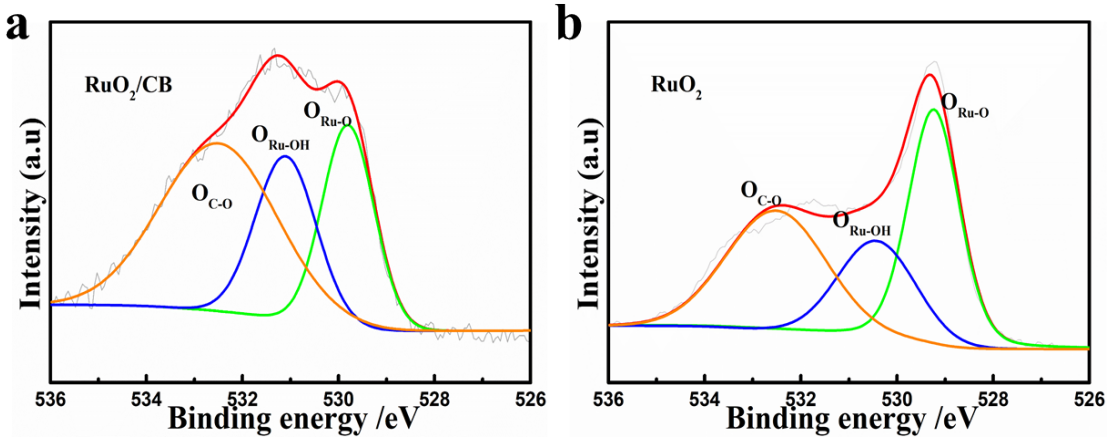

Fig. S6 High-resolution XPS spectra of O 1s in RuO_2/CB and RuO_2.

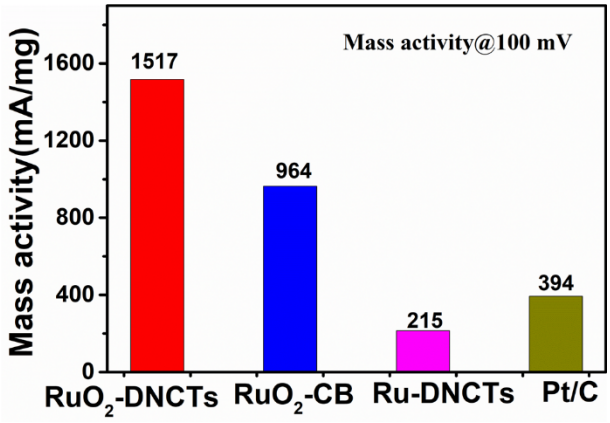

Fig. S7 Mass activity of HER performances for RuO_2-DNCTs, Ru-DNCTs, RuO_2/CB and Pt/C.

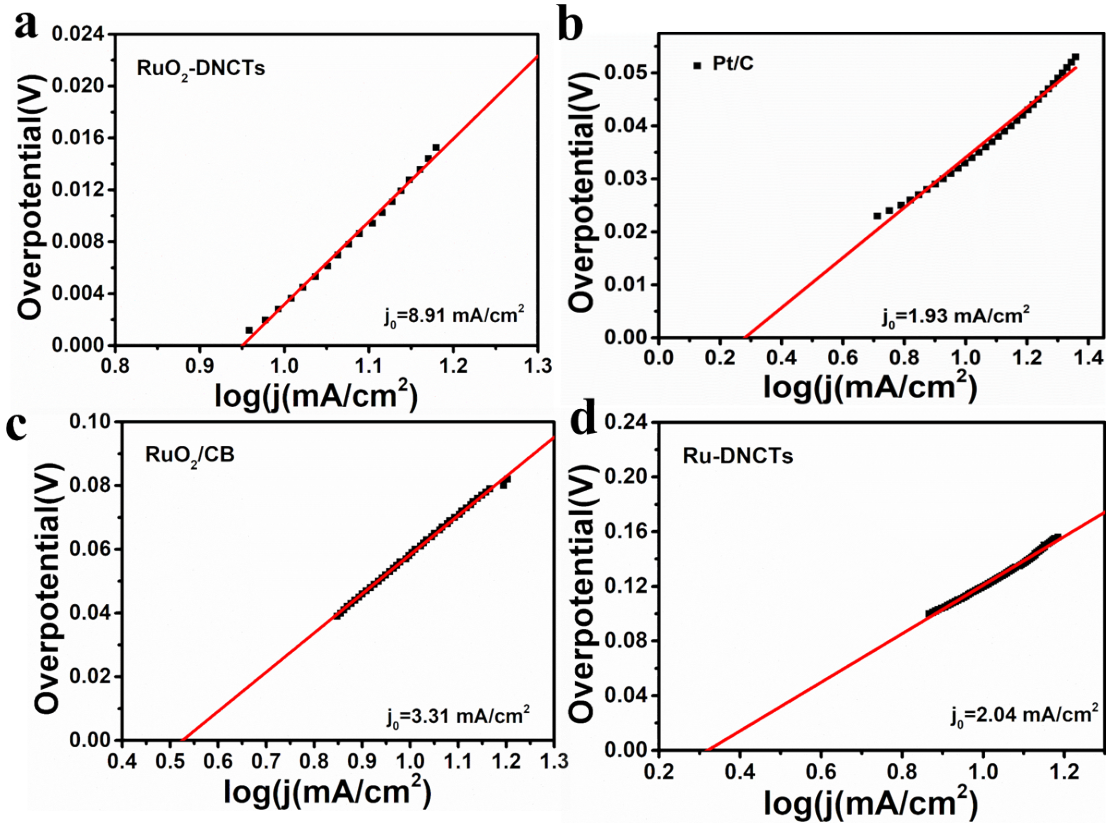

Fig. S8 (a-d) Exchange current densities (j_0) of RuO_2-DNCTs, Pt/C, RuO_2/CB and Ru-DNCTs.

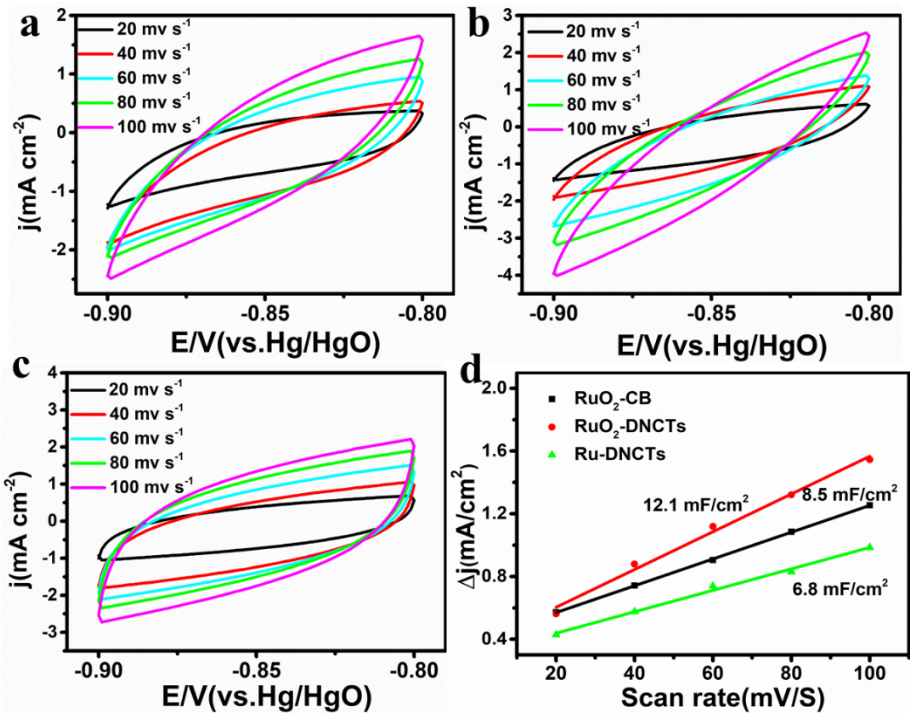

Fig. S9 (a-c) Cyclic voltammogram (CV) curves at different scan rates for RuO_2/DCNTs, RuO_2/CB and Ru/DCNTs. (d) The current density variation at 0.389 V versus RHE plotted against with the scan rates.

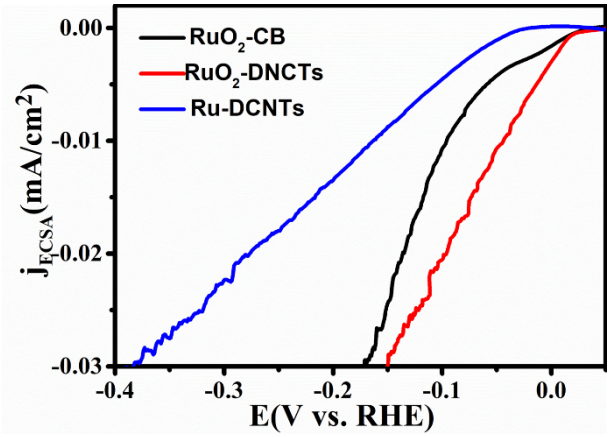

Fig.S10 ECSA normalized HER polarization curves of the as-prepared RuO_2-DCNTs, RuO_2/CB and Ru-DCNTs electrocatalysts.

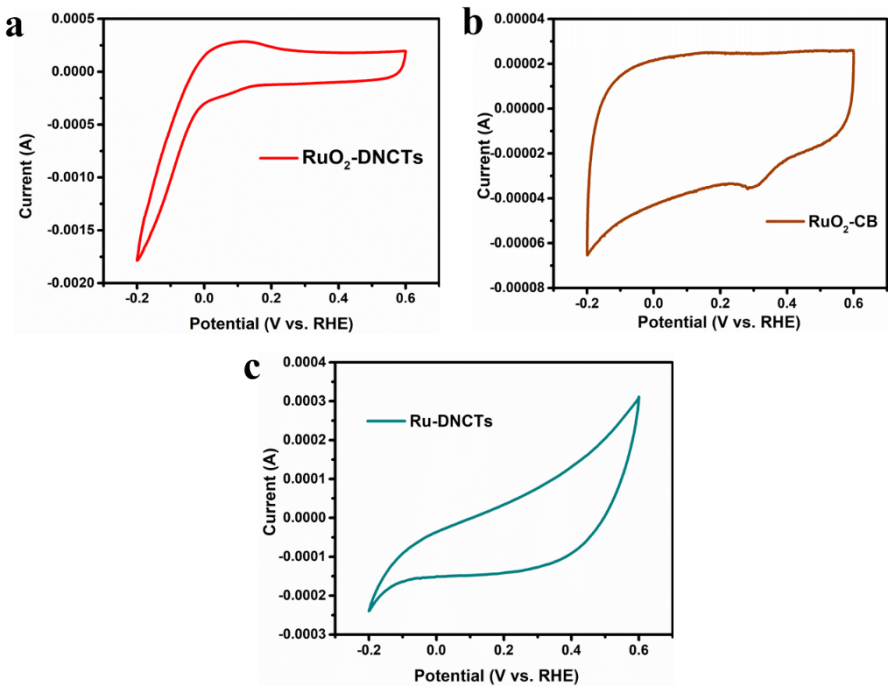

Fig. S11 Cyclic voltammogram (CV) curves of (a) RuO_2-DNCTs, (b) RuO_2/CB and (c) Ru-DNCTs in 1 M PBS (pH = 7) with a scan rate of 50 mV s^{-1}.

According to the formula described in the experimental section: $n = Q/2F = It/2F = IV/2Fv$, the number of active sites for RuO_2-DNCTs, RuO_2/CB and Ru- DNCTs is calculated to be $2.91952e^{-8}$ mol, $4.53e^{-9}$ mol and $1.22783e^{-8}$ mol, respectively, indicating that RuO_2-DNCTs catalyst has more abundant active sites than RuO_2/CB and Ru-DNCTs, respectively.

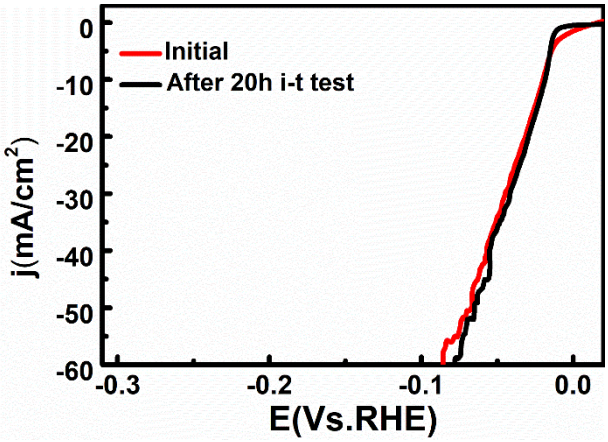

Fig. S12 LSV curves obtained initial and after 20 h i-t test for RuO_2-DCNTs.

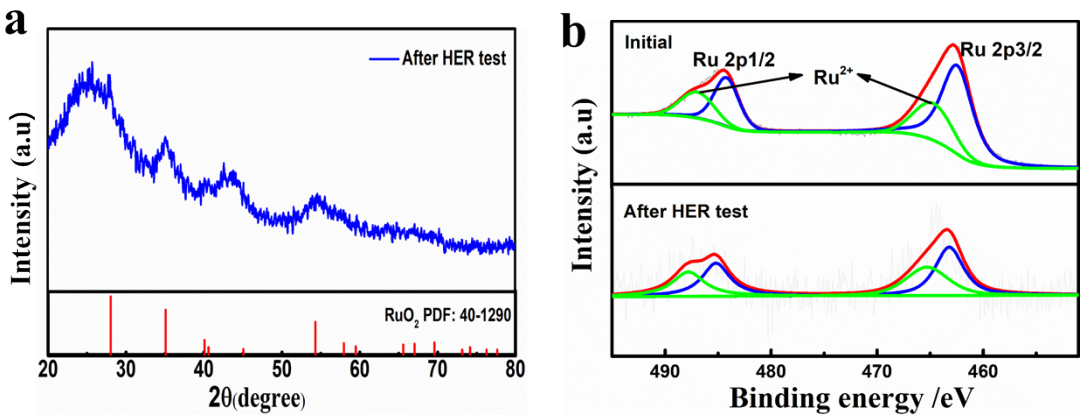

Fig. S13 X-ray diffraction pattern (XRD) and high-resolution XPS spectra of Ru 2p in RuO_2-DNCTs after HER

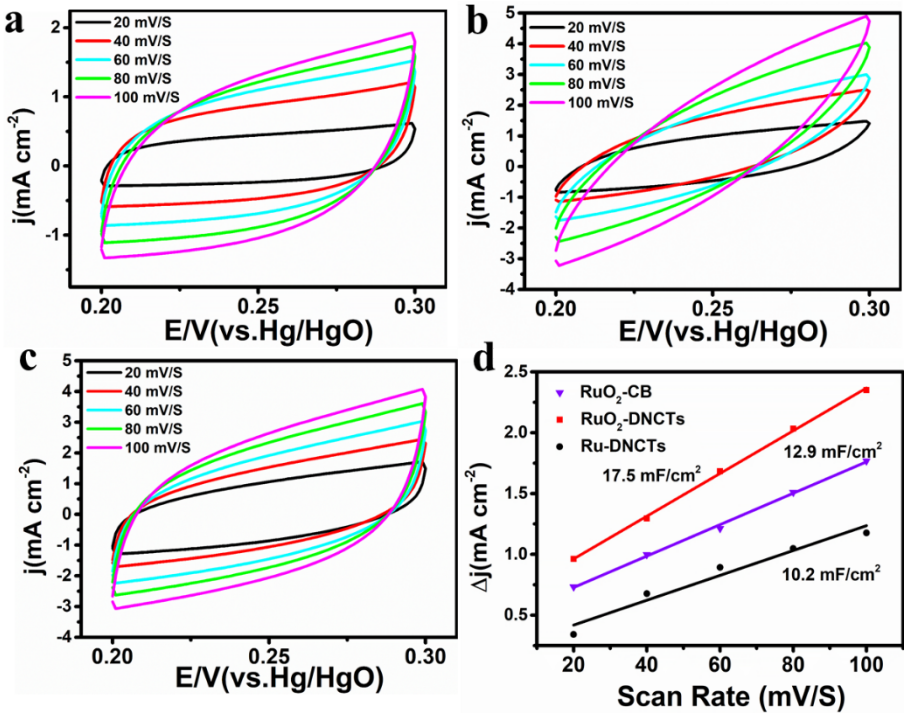

Fig. S14 (a-c) Cyclic voltammogram (CV) curves at different scan rates for RuO_2-DNCTs, RuO_2/CB and Ru-DNCTs, (d) The current density variation at 0.389 V versus RHE plotted against with the scan rates.

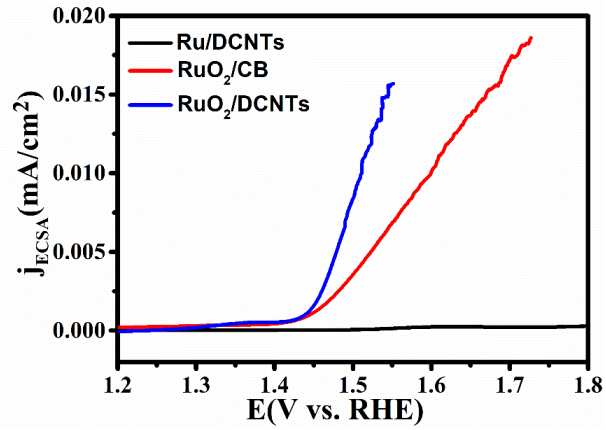

Fig. S15 The ECSA normalized OER polarization curves of the as-prepared RuO_2-DNCTs, RuO_2/CB and Ru-DNCTs electrocatalysts.

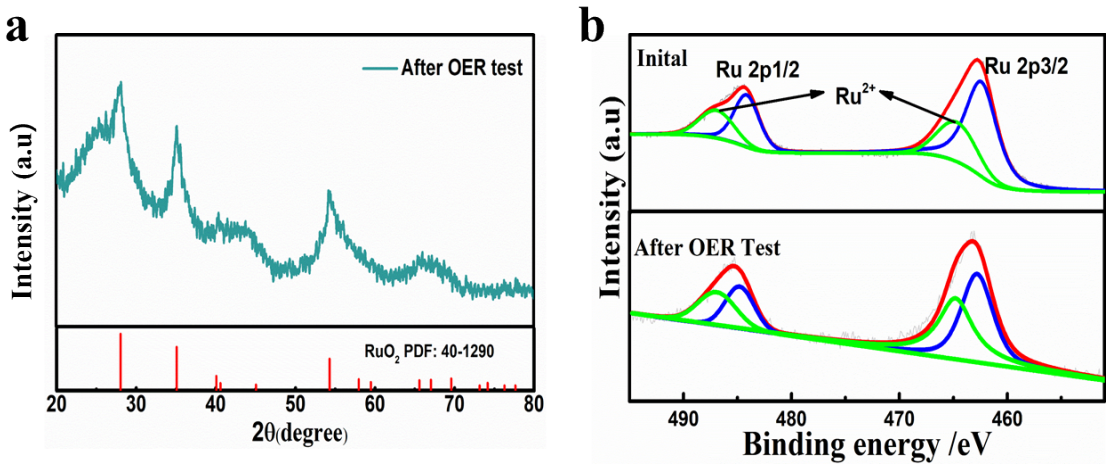

Fig. S16 X-ray diffraction pattern (XRD) and high-resolution XPS spectra of Ru 2p in RuO_2-DNCTs after OER(c-d) test.

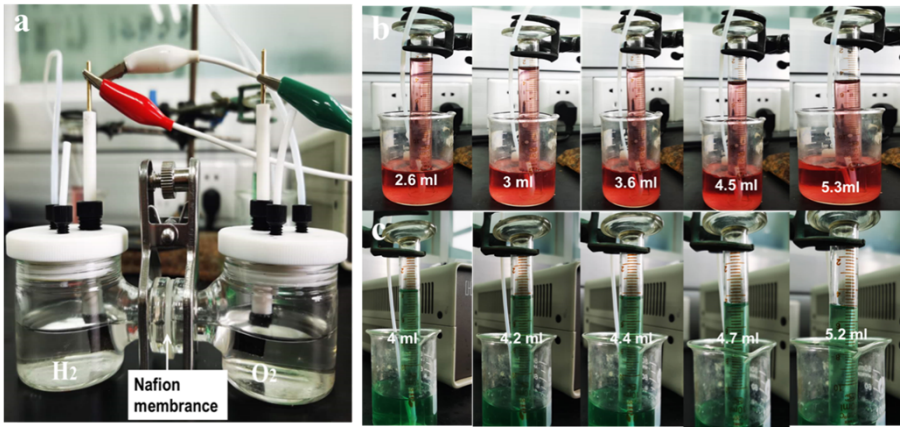

Fig. S17 (a) Gas collection device of water splitting, (b)Photographs of hydrogen and oxygen collected at different times.

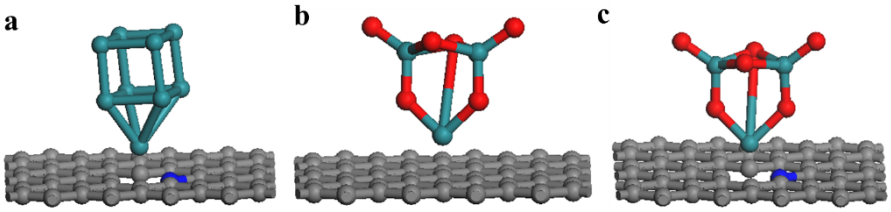

Fig. S18 (a-c)Calculated model of Ru-DNC, RuO_2-C and RuO_2-DNC.

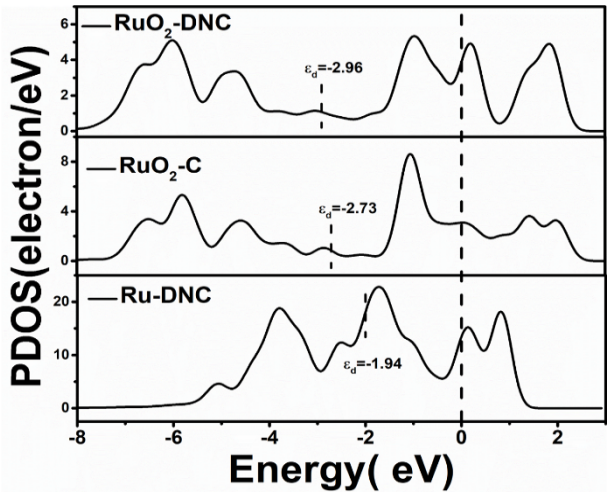

Fig. S19 Partial electronic density of states of Ru d orbital in RuO_2-DNC, RuO_2-C and Ru-DNC.

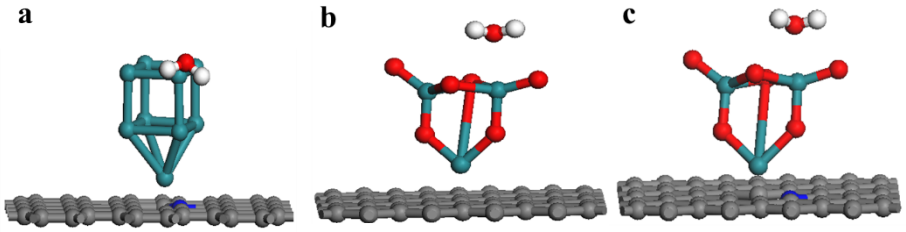

Fig. S20 Calculated model of H_2O on (a)Ru-DNC, (b)RuO_2-C and (c)RuO_2-DNC.

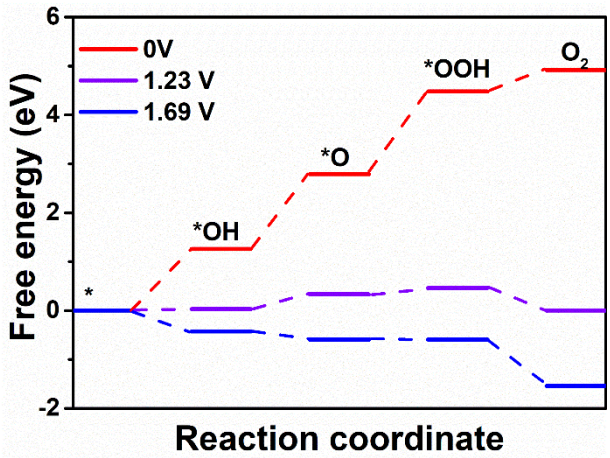

Fig. S21 Free-energy diagrams of RuO_2-DNC at different potential.

Table S1. HER comparison in 1.0 M KOH with the recently reported literatures

Materials	j(mA/m^2)	HER(mV)	Reference
RuO_2-DNCTs	10	19	**This work**
RuO_2/N-C	10	40	5
Ru_{40}@mONC	10	28	6
Ru/Ni_3N–Ni	10	53	7
RuNi-NCNFs	10	49	8
RuO_2-RuP_2/Ru	10	33	9
PtSA-$Co(OH)_2$@AgNWs	10	29	10
IrP_2@NC	10	28	11
Pd_3Ru/C	10	42	12
RuAu SAAs	10	24	13
CF@Ru-CoCH	10	66	14
NiRu@N–C	10	32	15
Ru-CoV-LDH/NF	10	32	16
Ru-NiFe-P	10	44	17
Ru-MnFeP/NF	10	35	18
MIL-53(Ru-NiFe)@NF	10	68	19

Table S2. C_{dl} and ECSA values of RuO_2-DNCTs, RuO_2-C and Ru-DNCTs in the region of (0.2)- (0.3) V versus Hg/HgO

Materials	**C_{dl}(mF/cm^2)**	ECSA(cm^2)
RuO_2-DNCTs	17.5	291
RuO_2-CB	12.9	215
Ru-DNCTs	10.2	170

Table S3. OER comparison in 1.0 M KOH with the recently reported literatures

Materials	j(mA/m^2)	OER(mV)	Reference
RuO_2-DNCTs	10	229	**This work**
$RuIrO_x$	10	250	20
RuO_2/N-C	10	280	5
RuCu NSs/C	10	230	21
D–RuO_2/TiO_2	10	296	22
Ru-CoV-LDH/NF	10	230	16
RuO_2/CeO_2	10	350	23
RuNi-NCNFs	10	290	8
Ru/RuO_2-MoO_2	10	260	24
CoNG/Ru	10	350	25
0.4-Ru@NG-750	10	372	26
Co doped RuO_2 NWs	10	304	27
Ir/MoS_2	10	330	28
Pt-MoS_2/CC	10	300	29

Table S4. Summary of overall water-splitting electrocatalysts

Materials	**Overpotential (V@10 mA/cm^2)**	Reference
RuO_2-DNCTs	1.48	This work
Ru-HMT-MP-7	1.50	9
D-RuO_2/TiO_2	1.59	22
RuO2/N–C	1.554	15
Ru/NiFe LDH-F/NF	1.53	30
NiRu@MWCNTs	1.51	31
Ru/Ni_3N–Ni	1.55	7
RuNi-NCNFs	1.564	8
CoNG/Ru	1.58	25
Ru_1Co_2 NP	1.59	32
Ru-NiCoP	1.515	33
OMS Mo2C/NC-Ru	1.62	34
Ru/RuO_2-MoO_2	1.54	35
RuCu NSs/C	1.49	21

Reference：

1 G. C. Xi, Y. K. Liu, X. Q. Wang, X. Y. Liu, Y. Y. Peng, Y. T. Qian, Large-scale synthesis, growth mechanism, and photoluminescence of ultrathin Te nanowires, *Cryst. Growth. Des.*, 2006, **6**, 2567-2570.

2 J. P. Perdew, K. Burke, M. Ernzerhof, Generalized gradient approximation made simple, *Phys. Rev. Lett.*, 1996, **77**, 3865-3868.

3 Y. C. Yao, S. L. Hu, W. X. Chen, Z. Q. Huang, W. C. Wei, T. Yao, R. R. Liu, K. T. Zang, X. Q. Wang, G. Wu, W. J. Yuan, T. W. Yuan, B. Q. Zhu, W. Liu, Z. J. Li, D. S. He, Z. G. Xue, Y. Wang, X. S. Zheng, J. C. Dong, C. R. Chang, Y. X. Chen, X. Hong, J. Luo, S. Q. Wei, W. X. Li, P. Strasser, Y. E. Wu, Y. D. Li, Engineering the electronic structure of single atom Ru sites via compressive strain boosts acidic water oxidation electrocatalysis, *Nat. Catal.*, 2019, **2**, 304-313.

4 D. Bahamon, M. Khalil, A. Belabbes, Y. Alwahedi, L. F. Vega, K. Polychronopoulou, A DFT study of the adsorption energy and electronic interactions of the SO_2 molecule on a CoP hydrotreating catalyst, *Rsc Adv.*, 2021, **11**, 2947-2957.

5 C. Z. Yuan, Y. F. Jiang, Z. W. Zhao, S. J. Zhao, X. Zhou, T. Y. Cheang, A. W. Xu, Molecule-Assisted Synthesis of Highly Dispersed Ultrasmall RuO_2 Nanoparticles on Nitrogen-Doped Carbon Matrix as Ultraefficient Bifunctional Electrocatalysts for Overall Water Splitting, *Acs Sustain. Chem. Eng.*, 2018, **6**, 11529-11535.

6 Q. F. Yang, B. T. Zhu, F. Wang, C. J. Zhang, J. H. Cai, P. Jin, L. Feng, Ru/NC heterointerfaces boost energy-efficient production of green H_2 over a wide pH range, *Nano Res.*, 2022, **15**, 5134-5142.

7 Z. Liu, M. Zha, Q. Wang, G. Hu, L. Feng, Overall water-splitting reaction efficiently catalyzed by a novel bi-functional Ru/Ni_3N–Ni electrode, *Chem Commoun.*, 2020, **56**, 2352-2355.

8 M. X. Li, H. Y. Wang, W. D. Zhu, W. M. Li, C. Wang, X. F. Lu, RuNi Nanoparticles Embedded in N-Doped Carbon Nanofibers as a Robust Bifunctional Catalyst for Efficient Overall Water Splitting, *Adv. Sci.*, 2020, **7**, 1901833.

9 Y. Zhao, X. Y. Zhang, Y. X. Gao, Z. Chen, Z. J. Li, T. Y. Ma, Z. X. Wu, L. Wang, S. H. Feng, Heterostructure of RuO_2-RuP_2/Ru Derived from HMT-based Coordination Polymers as Superior pH-Universal Electrocatalyst for Hydrogen Evolution Reaction, *Small*, 2022, **18**, 2105168.

10 K. L. Zhou, C. H. Wang, Z. L. Wang, C. B. Han, Q. Q. Zhang, X. X. Ke, J. B. Liu, H. Wang, Seamlessly conductive $Co(OH)_2$ tailored atomically dispersed Pt electrocatalyst with a hierarchical nanostructure for an efficient hydrogen evolution reaction, *Energy Environ. Sci.*, 2020, **13**, 3082-3092.

11 Z. H. Pu, J. H. Zhao, I. S. Amiinu, W. Q. Li, M. Wang, D. P. He, S. C. Mu, A universal synthesis strategy for P-rich noble metal diphosphide-based electrocatalysts for the hydrogen evolution reaction, *Energy Environ. Sci.*, 2019, **12**, 952-957.

12 X. P. Qin, L. L. Zhang, G. L. Xu, S. Q. Zhu, Q. Wang, M. Gu, X. Y. Zhang, C. J. Sun, P. B. Balbuena, K. Amine, M. H. Shao, The Role of Ru in Improving the Activity of Pd toward Hydrogen Evolution and Oxidation Reactions in Alkaline Solutions, *Acs Catal.*, 2019, **9**, 9614-9621.

13 C. H. Chen, D. Y. Wu, Z. Li, R. Zhang, C. G. Kuai, X. R. Zhao, C. K. Dong, S. Z. Qiao, H. Liu, X. W. Du, Ruthenium-Based Single-Atom Alloy with High Electrocatalytic Activity for Hydrogen Evolution, *Adv. Energy Mater.*, 2019, **9**, 1803913.

14 J. C. Li, Q. W. Zhou, Z. H. Shen, S. W. Li, J. Pu, C. L. Zhong, M. Q. Cao, X. Jin, H. G. Zhang, Y. Y. Wang, H. X. Ma, Synergistic effect of ultrafine nano-Ru decorated cobalt carbonate hydroxides nanowires for accelerated alkaline hydrogen evolution reaction, *Electrochim. Acta.*, 2020, **331**, 135367.

15 Y. Xu, S. L. Yin, C. J. Li, K. Deng, H. R. Xue, X. N. Li, H. J. Wang, L. Wang, Low-ruthenium-content NiRu nanoalloys encapsulated in nitrogen-doped carbon as highly efficient and pH-universal electrocatalysts for the hydrogen evolution reaction, *J Mater. Chem. A*, 2018, **6**, 1376-1381.

16 W. Li, B. M. Feng, L. Y. Yi, J. Y. Li, W. H. Hu, Highly Efficient Alkaline Water Splitting with Ru-Doped Co-V Layered Double Hydroxide Nanosheets as a

Bifunctional Electrocatalyst, *ChemSusChem*, 2021, **14**, 730-737.

17 M. J. Qu, Y. M. Jiang, M. Yang, S. Liu, Q. F. Guo, W. Shen, M. Li, R.X. He, Regulating electron density of NiFe-P nanosheets electrocatalysts by a trifle of Ru for high-efficient overall water splitting, *Appl. Catal. B-Environ.*, 2020, **263**, 118324.

18 D. Chen, Z. H. Pu, R. H. Lu, P. X. Ji, P. Y. Wang, J. W. Zhu, C. Lin, H. W. Li, X. G. Zhou, Z. Y. Hu, F. J. Xia, J. S. Wu, S. C. Mu, Ultralow Ru Loading Transition Metal Phosphides as High-Efficient Bifunctional Electrocatalyst for a Solar-to-Hydrogen Generation System, *Adv. Energy Mater.*, 2020, **10**, 2000814.

19 M. Zhao, H. L. Li, W. Li, J. Y. Li, L.Y. Yi, W. H. Hu, C. M. Li, Ru-Doping Enhanced Electrocatalysis of Metal-Organic Framework Nanosheets toward Overall Water Splitting, *Chem-Eur. J*, 2020, **26**, 17091-17096.

20 Z. W. Zhuang, Y. Wang, C. Q. Xu, S. J. Liu, C. Chen, Q. Peng, Z. B. Zhuang, H. Xiao, Y. Pan, S. Q. Lu, R. Yu, W. C. Cheong, X. Cao, K. L. Wu, K. A. Sun, D. S. Wang, J. Li, Y. D. Li, Three-dimensional open nano-netcage electrocatalysts for efficient pH-universal overall water splitting, *Nat. Commun.*, 2019, **10**, 4875.

21 Q. Yao, B.L. Huang, N. Zhang, M.Z. Sun, Q. Shao, X.Q. Huang, Channel-Rich RuCu Nanosheets for pH-Universal Overall Water Splitting Electrocatalysis, Angew *Chem. Int. Edit.*, 2019, **58**, 13983-13988.

22 W. Q. Li, H. Zhang, M. Z. Hong, L. L. Zhang, X. Feng, M. F. Shi, W. X. Hu, S. C. Mu, Defective RuO_2/TiO_2 nano-heterostructure advances hydrogen production by electrochemical water splitting, *Chem. Eng. J*, 2022, **431**, 134072.

23 S. M. Galani, A. Mondal, D. N. Srivastava, A. B. Panda, Development of RuO_2/CeO_2 heterostructure as an efficient OER electrocatalyst for alkaline water splitting, *Int. J Hydrogen Energ.*, 2020, **45**, 18635-18644.

24 Y. X. Fan, X. D. Zhang, Y. J. Zhang, X. Xie, J. Ding, J. L. Cai, B. J. Li, H. L. Lv, L. Y. Liu, M. M. Zhu, X. C. Zheng, Q. Cai, Y. S. Liu, S. Y. Lu, Decoration of Ru/RuO_2 hybrid nanoparticles on MoO_2 plane as bifunctional electrocatalyst for overall water splitting, *J Colloid Interf. Sci.*, 2021, **604**, 508-516.

25 T. He, Y. Peng, Q.X. Jia, J.E. Lu, Q.M. Liu, R. Mercado, Y. Chen, F. Nichols, Y.

Zhang, S.W. Chen, Nanocomposites Based on Ruthenium Nanoparticles Supported on Cobalt and Nitrogen-Codoped Graphene Nanosheets as Bifunctional Catalysts for Electrochemical Water Splitting, *Acs Appl. Mater. Inter.*, 2019, **11**, 46912-46919.

26 L. Bai, Z. Y. Duan, X. D. Wen, R. Si, Q. Q. Zhang, J. Q. Guan, Highly Dispersed Ruthenium-Based Multifunctional Electrocatalyst, *Acs Catal.*, 2019, **9**, 9897-9904.

27 J. Wang, Y. J. Ji, R. G. Yin, Y. Y. Li, Q. Shao, X. Q. Huang, Transition metal-doped ultrathin RuO_2 networked nanowires for efficient overall water splitting across a broad pH range, *J Mater. Chem. A*, 2019, **7**, 6411-6416.

28 X. P. Han, X. Y. Wu, Y. D. Deng, J. Liu, J. Lu, C. Zhong, W. B. Hu, Ultrafine Pt Nanoparticle-Decorated Pyrite-Type CoS_2 Nanosheet Arrays Coated on Carbon Cloth as a Bifunctional Electrode for Overall Water Splitting, *Adv. Energy Mater.*, 2018, **8** , 1800935.

29 S. T. Wei, X. Q. Cui, Y. C. Xu, B. Shang, Q. H. Zhang, L. Gu, X. F. Fan, L. R. Zheng, C. M. Hou, H. H. Huang, S. S. Wen, W. T. Zheng, Iridium-Triggered Phase Transition of MoS_2 Nanosheets Boosts Overall Water Splitting in Alkaline Media, *ACS Energy Lett.*, 2019, **4**, 368-374.

30 J. Q. Chi, X. Y. Zhang, X. Ma, B. Dong, J. Q. Zhang, B. Y. Guo, M. Yang, L. Wang, Y. M. Chai, C. G. Liu, Interface Charge Engineering of Ultrafine Ru/Ni_2P Nanoparticles Encapsulated in N,P-Codoped Hollow Carbon Nanospheres for Efficient Hydrogen Evolution, *ACS Sustain. Chem. Eng.*, 2019, **7**, 17714-17722.

31 Z. K. Peng, J. M. Liu, B. Hu, Y.P. Yang, Y. Q. Guo, B. J. Li, L. Li, Z. H. Zhang, B. B. Cui, L. H. He, M. Du, Surface Engineering on Nickel-Ruthenium Nanoalloys Attached Defective Carbon Sites as Superior Bifunctional Electrocatalysts for Overall Water Splitting, *Acs Appl. Mater. Inter.*, 2020, **12**, 13842-13851.

32 Y. K. Bao, J. Y. Dai, J. Zhao, Y. Wu, C. Li, L. F. Ji, X. Zhang, F. C. Yang, Modulation in Ruthenium-Cobalt Electronic Structure for Highly Efficient Overall Water Splitting, *Acs Appl. Energy Mater.*, 2020, **3**, 1869-1874.

33 K. Yang, P. P. Xu, Z. Y. Lin, Y. Yang, P. Jiang, C. L. Wang, S. Liu, S. P. Gong, L. Hu, Q. W. Chen, Ultrasmall Ru/Cu-doped RuO_2 Complex Embedded in

Amorphous Carbon Skeleton as Highly Active Bifunctional Electrocatalysts for Overall Water Splitting, *Small*, 2018, **14**, 1803009.

34 K. X. Wang, S. Wang, K. S. Hui, H. X. Gao, D. A. Dinh, C. Z. Yuan, C. Y. Zha, Z. P. Shao, Z. K. Tang, K. N. Hui, Synergistically boosting the elementary reactions over multiheterogeneous ordered macroporous Mo_2C/NC-Ru for highly efficient alkaline hydrogen evolution, *Carbon Energy*, 2022, **4**, 856-866.

35 Y. Fan, X. Zhang, Y. Zhang, X. Xie, J. Ding, J. Cai, B. Li, H. Lv, L. Liu, M. Zhu, Decoration of Ru/RuO_2 hybrid nanoparticles on MoO_2 plane as bifunctional electrocatalyst for overall water splitting, *J Colloid Interf. Sci.*, 2021, **604**, 508-516.